J. Fluid Mech. (2003), vol. 496, pp. 165–192. © 2003 Cambridge University Press
DOI: 10.1017/S0022112003006402 Printed in the United Kingdom

Tsunami scour around a cylinder

By SUSAN TONKIN,[1] HARRY YEH,[2] FUMINORI KATO[3] AND SHINJI SATO[4]

[1]Moffatt & Nichol Engineers, 710 Second Ave #720, Seattle, WA 98104, USA

[2]Department of Civil Engineering, Oregon State University, Corvallis, OR 97331, USA

[3]National Institute for Land and Infrastructure Management, 1 Asahi, Tsukuba City, Ibaraki 305-804, Japan

[4]Department of Civil Engineering, University of Tokyo, Hongo 7-3-1, Bunkyo-ku, Tokyo 113-8656, Japan

(Received 8 October 2001 and in revised form 14 July 2003)

A series of scale-model experiments investigated the scouring mechanisms associated with a tsunami impinging on a coastal cylindrical structure. Since scaling effects are significant in sediment transport, a large-scale sediment tank was used. Video images from inside the cylinder elucidated the vortex structures and the time development of scour around the cylinder. The scour development and mechanisms differed according to the sediment substrate – sand or gravel. For gravel, the most rapid scour coincided with the greatest flow velocities. On the other hand, for the sand substrate, the most rapid scour occurred at the end of drawdown – after flow velocities had subsided and shear stresses were presumed to have decreased. This behaviour can be explained in terms of pore pressure gradients. As the water level and velocity subside, the pressure on the sediment bed decreases, creating a vertical pressure gradient within the sand and decreasing the effective stress within the sand. Gravel is too porous to sustain this pressure gradient. During drawdown, the surface pressure decreases approximately linearly from a sustained peak at ΔP to zero over time ΔT. The critical fraction Λ of the buoyant weight of sediment supported by the pore pressure gradient can be estimated as

$$\Lambda = \frac{2}{\sqrt{\pi}} \frac{\Delta P}{\gamma_b \sqrt{c_v \Delta T}},$$

in which γ_b is the buoyant specific weight of the saturated sediment and c_v is the coefficient of consolidation. Much deeper scour was observed where Λ exceeded one-half.

1. Introduction

It is known that tsunami attack causes substantial erosion and scour on shorelines. For example, the 1960 Chilean Tsunami scoured out the port entrance by more than 10 m at Kesen-numa in Japan (Takahashi, Imamura & Shuto 1992). Several tsunami surveys performed from the 1992 Nicaragua tsunami to the 1998 Papua New Guinea tsunami also discovered substantial tsunami scouring effects around structures and trees. It appears probable that the scouring mechanisms associated with tsunami runup are different from those in a steady current (such as a river bridge-pier environment) or in a consistent short-wave field (such as an offshore pier environment). This is because tsunami scouring occurs in transient flow (duration less than an hour).

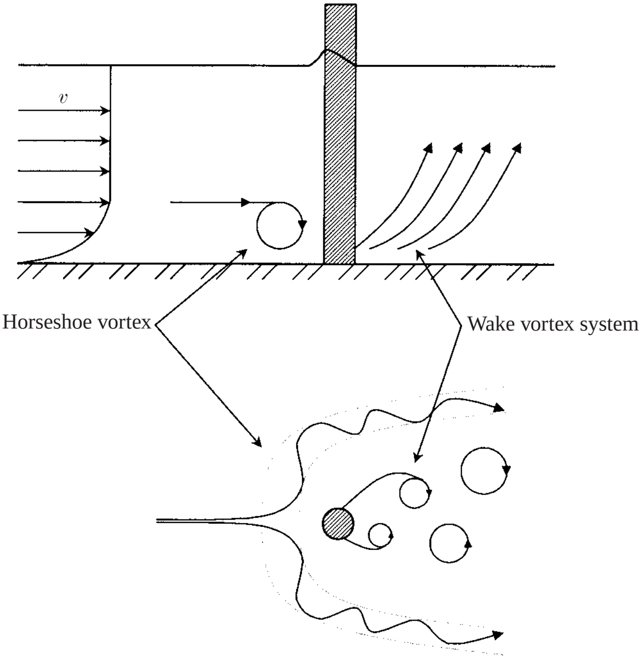

Figure 1. A schematic view of the vortex system around a pier in a steady current (after Dey 1999).

The subject of local scour around cylindrical piers in a steady current and, more recently, combined waves and currents, has been extensively studied. Breusers, Nicolet & Shen (1977) quote 90 references in their review paper, and the publication rate has not slowed.

Most modelling of bridge-pier scour has used the shear stress approach: scour is assumed to occur if the shear stress induced by fluid motion near the base of the structure exceeds the critical value defined through the Shields diagram (e.g. Hoffmans & Verheij 1997). High shear stresses and extensive scouring are caused by the vortices surrounding bridge piers. There are two main vortex structures: the horseshoe vortex upstream of the pier, and the downstream wake-vortex system. The main scour hole forms upstream of the pier, beneath the horseshoe vortex, which sinks into the hole as scouring progresses. Figure 1 is a sketch of this vortex system. In practice, even in the steady state, the vortex system is much more complicated than this (e.g. Baker 1979; DePonte & Monti 1995).

In a wave field, the equilibrium scour depth is generally less than the steady-current value. The scour depth is modified by a dependence on the Keulegan–Carpenter number (e.g. Sumer & Fredsøe 1999) and possibly on the Ursell number (Çevik & Yüksel 1999).

In a transient situation – such as a tsunami or storm surge attack on a coastal structure – the quasi-equilibrium approach developed for bridge piers is less appropriate. In a transient situation, pressure can build up in the water-filled pores within the sediment bed. This pore water pressure (strictly, the vertical gradient in the pore pressure) pushes the sediment grains apart, decreasing the vertical effective stress between the grains. The frictional force between the grains is proportional to the vertical effective stress. Once the effective stress has dropped to zero, the sediment acts like a liquid – there are essentially no frictional forces keeping the sediment grains at rest under shear stresses. Scour can occur very rapidly under such a condition. In the present scale-model experiments, the most rapid scouring occurs at the very end of the drawdown, when the pore pressure gradient is likely to be greatest. This scour mechanism is better described using the concepts of pore pressure build-up and consequent loss of shear strength around the structure, rather than in terms of gradual pickup of sediment particles as a result of localized shear stress.

Terzaghi (1925, 1956) developed much of the basic theory describing the propagation of excess pore pressures in fine soils, and applied the concept to submarine slope failures as a result of sediment build-up and high tidal ranges. Madsen (1978), Okusa (1985) and Jeng & Hsu (1996) extended this theory to compressible fluids. Madsen showed that the combination of shear strength reduction as a result of excess pore pressures, and shear stress as a result of the wave-induced bottom currents, could cause failure of a clay or mud bed. Sumer, Whitehouse & Tørum (2001) further investigated the influence of pore pressures on scour of fine soils caused by short waves (i.e. cyclic loading).

Baird, Mason & Horn (1996) tested a model of water table elevations in sandy beaches. They noted that the pore pressure release associated with backwash could induce liquefaction of the beach surface. Mia & Nago (2000) carried out small-scale model experiments to demonstrate excess scour associated with a sudden drop in pressure (flood level) behind a bridge pier, and attributed this to sediment liquefaction.

In this paper, we describe a series of scale model experiments performed to investigate the scouring mechanisms associated with tsunami runup onto a beach. Section 2 describes the experimental setup, and § 3 the observations of flow patterns, temporal development of the scour hole, and the pore pressures within the sediment bed. Conclusions regarding the dominant mechanism and a model for the extent of the deepest scour hole, based upon the release of pore pressures at the end of drawdown, are given in § 4.

2. Experimental setup

The scaling effects of small-scale laboratory scouring experiments are probably significant, since normally the sand substrate must be modelled at full scale while the wave and structures are modelled at reduced scale. Very fine sediments cannot be used as a scale model of sand, since finer sediments tend to become cohesive. A large-scale sediment tank was therefore used to reduce scaling effects (135 m long, 2 m wide, and 5 m deep). A solitary wave was generated offshore as a model of a tsunami incident on a beach; based on the runup heights (discussed later), this model can be considered as about one-tenth of prototype scale for a 'typical' tsunami.

Figure 2 illustrates the experimental setup. A beach of well-graded sand was constructed with a uniform slope of 1:20. Table 1 shows the measured sand characteristics (Tokyo Soil Research 1999); the bulk density of the saturated sand calculated from the mean grain density and the mean voids ratio is $\rho_{sat} = 1.93 \times 10^3\,\mathrm{kg\,m^{-3}}$.

The model cylinder shown in figure 3 was placed upright on the beach. The cylinder was 50 cm in diameter, made of 1 cm thick Plexiglas, water tight at the bottom end, and connected above to an aluminium cylinder for stiffness. In some experiments a gravel collar ($D_{50} = 3.6$ mm) surrounded the buried cylinder to a thickness of 25 cm and a depth of 25 cm beneath the cylinder; see figure 3. At the front, side and back of the cylinder, and between the cylinder and the sidewall, the water surface

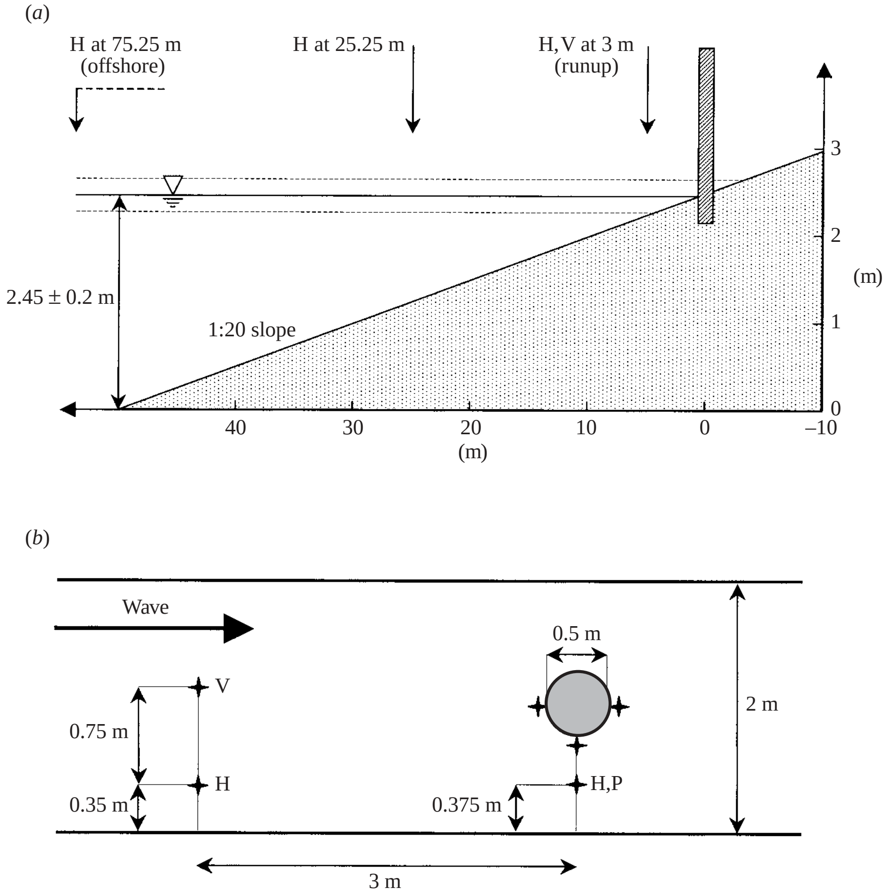

FIGURE 2. Schematics of the experimental setup: (*a*) elevation view, (*b*) plan view. The beach is constructed of well-graded sand. 'H' and 'V' indicate the locations of the wave gauges (height) and flow meter (velocity), respectively. Pore pressure transducers and wave gauges are installed at the locations marked with '✢' around the cylinder.

Quantity	Symbol	Value
Sediment grain density (kg m^{-3})	ρ_s	2.643×10^3
Median grain size (mm)	D_{50}	0.35
Natural water content (%)	w_n	17.2
Voids ratio	e_0	0.767
Permeability (m s^{-1})	k	0.493×10^{-3}

TABLE 1. Measured sand parameters.

elevation was measured with a 60 cm long capacitance-type wave gauge. Pore pressure transducers (2.0 cm in diameter, 0–50 kPa pressure range, no more than 0.2 s response time) were placed at the same four locations in the channel, at 10 cm, 20 cm and 30 cm below the initial level of the beach surface. The wave height was measured at 75.75 m, 25.25 m and 3 m offshore from the cylinder. The vertical and cross-shore velocity components were measured at 7.5 cm above the beach surface at 3 m offshore

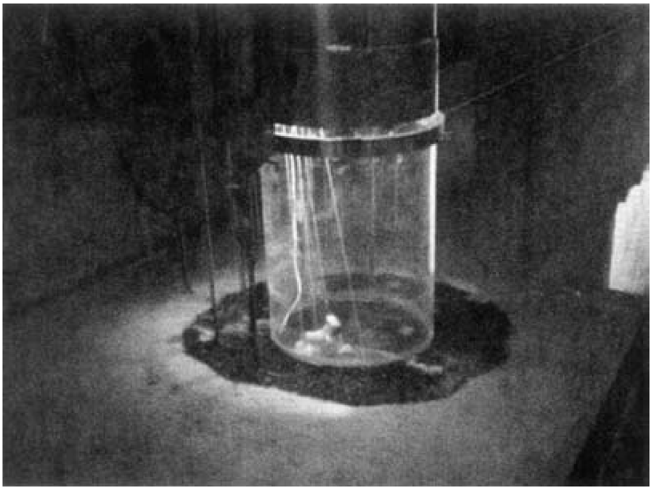

FIGURE 3. Cylinder surrounded by a gravel collar.

from the cylinder using an electromagnetic flow meter (2.0 cm in diameter, $\pm 2\,\mathrm{m\,s^{-1}}$ velocity range with less than 0.2 s response time).

Three miniature CCD cameras were located inside the cylinder, facing out, to record the scour process; the three cameras combined provided more than 180° field of view. Video cameras also recorded the experiment through the transparent glass sidewall of the flume and from above. The scouring process was observed using the video cameras throughout the wave runup and drawdown, and correlated with the wave and pressure characteristics.

Solitary waves were generated by a piston-type wavemaker driven by a large servomotor; the maximum stroke of the wave paddle was 2.4 m with a maximum speed of $1.11\,\mathrm{m\,s^{-1}}$. The paddle was capable of generating a clean solitary wave close to the theoretical wave form, at least 40 cm height in 3 m water depth.

A series of 18 scour experiments was performed. The following parameters were varied:

(i) The still water depth h (2.25 m, 2.45 m or 2.65 m). Since the cylinder location in the tank was fixed, the different still water depths corresponded to a cylinder that was initially 4 m onshore, on the shoreline, or 4 m offshore.

(ii) The incident wave height H (approximately 10 cm, 20 cm or 30 cm), chosen to give H/h equal to 0.05, 0.09 or 0.13. The 10 cm waves were non-breaking; the 20 and 30 cm waves were breaking at the shoreline.

(iii) The depth to which the cylinder was buried (20 cm, 37 cm or 50 cm);

(iv) The presence or absence of a gravel collar.

Two further experiments were carried out with no cylinder present, to check that the cylinder did not grossly change the wave runup characteristics and that the sidewalls were not close enough to the cylinder to significantly change flow characteristics at the cylinder. Figure 4 shows the measured runup heights both with and without a cylinder present: the presence of a cylinder does not significantly change the runup height. Synolakis' (1987) experiments investigated runup characteristics for a solitary wave on an inclined beach, with no blocking. The runup wave fronts in Synolakis' experiments had a parabolic shape in plan view (presumably due to sidewall effects), so he differentiated between the maximum and the average runup for a given wave.

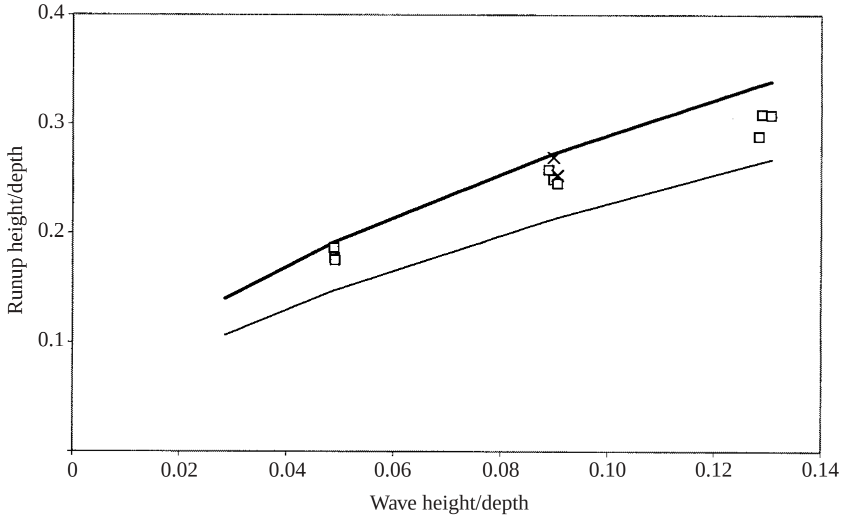

FIGURE 4. Measured runup heights compared with Synolakis' curves for breaking runup heights. Squares, measured values with the cylinder present; crosses, measured values with the cylinder absent; thick line, maximum runup height for breaking waves observed by Synolakis (1987); thin line, average runup height for breaking waves observed by Synolakis. Synolakis' experiments investigated runup characteristics for a solitary wave on an inclined beach, with no blocking. The runup wave fronts in Synolakis' experiments had a parabolic shape in plan view (presumably due to sidewall effects), so he differentiated between the maximum and the average runup for a given wave.

The present results lie well within the limits defined by Synolakis' experimental curves.

Additional evidence that the sidewalls did not greatly affect the flow near the cylinder is given by the final scour depths and patterns, presented in Yeh, Kato & Sato (2001); figure 5 shows one example (Case I, see below). The scour hole extends less than half-way from the cylinder to the wall, suggesting that the local scour is affected little by the wall. This is not to claim complete elimination of sidewall influence; for example, the wake formation behind the cylinder might have been altered if no sidewalls were present.

3. Observations

The rates and mechanisms of scouring are greatly elucidated by the video images taken from inside and around the cylinder. This section compares three experiment cases:

(I) Sand substrate, cylinder initially at the shoreline, water depth $h = 2.45\,\text{m}$, offshore incident wave height $H = 22\,\text{cm}$, $H/h = 0.09$.

(II) Gravel substrate, cylinder initially at the shoreline, water depth $h = 2.45\,\text{m}$, offshore incident wave height $H = 22\,\text{cm}$, $H/h = 0.09$.

(III) Sand substrate, cylinder initially in 20 cm water depth, water depth $h = 2.65\,\text{m}$, offshore incident wave height $H = 34\,\text{cm}$, $H/h = 0.13$.

The first two cases are identical, apart from a gravel collar around the cylinder in Case II (see figure 3). Case III illustrates differences in the runup vortex structure that can arise from differences in the incident wave and the cylinder location.

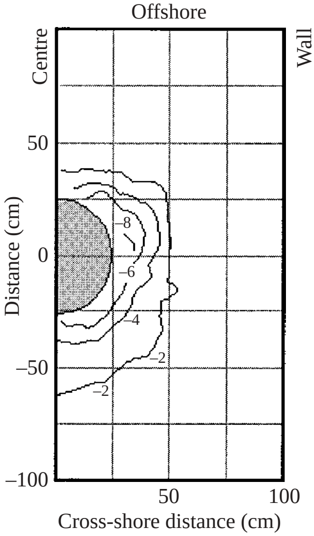

FIGURE 5. Final scour depth for Case I, cylinder embedded in sand at the shoreline with a 22 cm incident wave. The contours are at 2 cm intervals, with little scour well away from the cylinder. The cylinder is shown as a grey half-circle. The scour hole is symmetrical around the centre of the tank, so only one side is shown.

3.1. *Case I, sand substrate: flow and scour observations*

Figure 6 illustrates the flow and scour behaviour for Case I: sand substrate, with the cylinder initially on the shoreline ($h = 2.45$ m) and the offshore incident wave height 22 cm ($H/h = 0.09$). Figure 6(*a*) shows a typical composite frame, taken at the initial wave impact ($t = 0$).

The two panels in the upper right-hand part of figure 6(*a*) were recorded from directly above the cylinder. The wave is running from left to right; it is breaking at the offshore side of the cylinder, at point A. There are two views of the same breaking wave because of the overlap between the fields of view of the two downward-looking cameras. The wake from the instruments (wave gauge and flow meter) 3 m offshore from the cylinder is visible as a slight surface disturbance.

The two lower panels were recorded from inside the cylinder. Each panel shows approximately a 90° horizontal field of view. Points A and C – corresponding to points A and C in the upper panels – are directly offshore and onshore. There is again a slight overlap between the two panels, such that point B – at the side of the cylinder – appears twice. The field of view of the two lower panels is about 30 cm vertically and about 40 cm each (80 cm or 180° total) horizontally.

The two vertical rods were used to place the miniature CCD video cameras on the bottom of the cylinder. The device at the base of each rod is a timing light, used to synchronize the visual data with other electronic data such as water-level variations.

The arrows in this and subsequent figures are used to illustrate the flow field. The top of the sediment layer is highlighted in figure 6(*a*); this initial sediment level will be indicated as a broken line in subsequent figures.

The upper left-hand panel is a side view. The cylinder is partly hidden by the breaking wave.

Points A and C coincide with pore pressure and wave height sensors at the front (offshore) and the back (onshore) of the cylinder. Point B is located diametrically

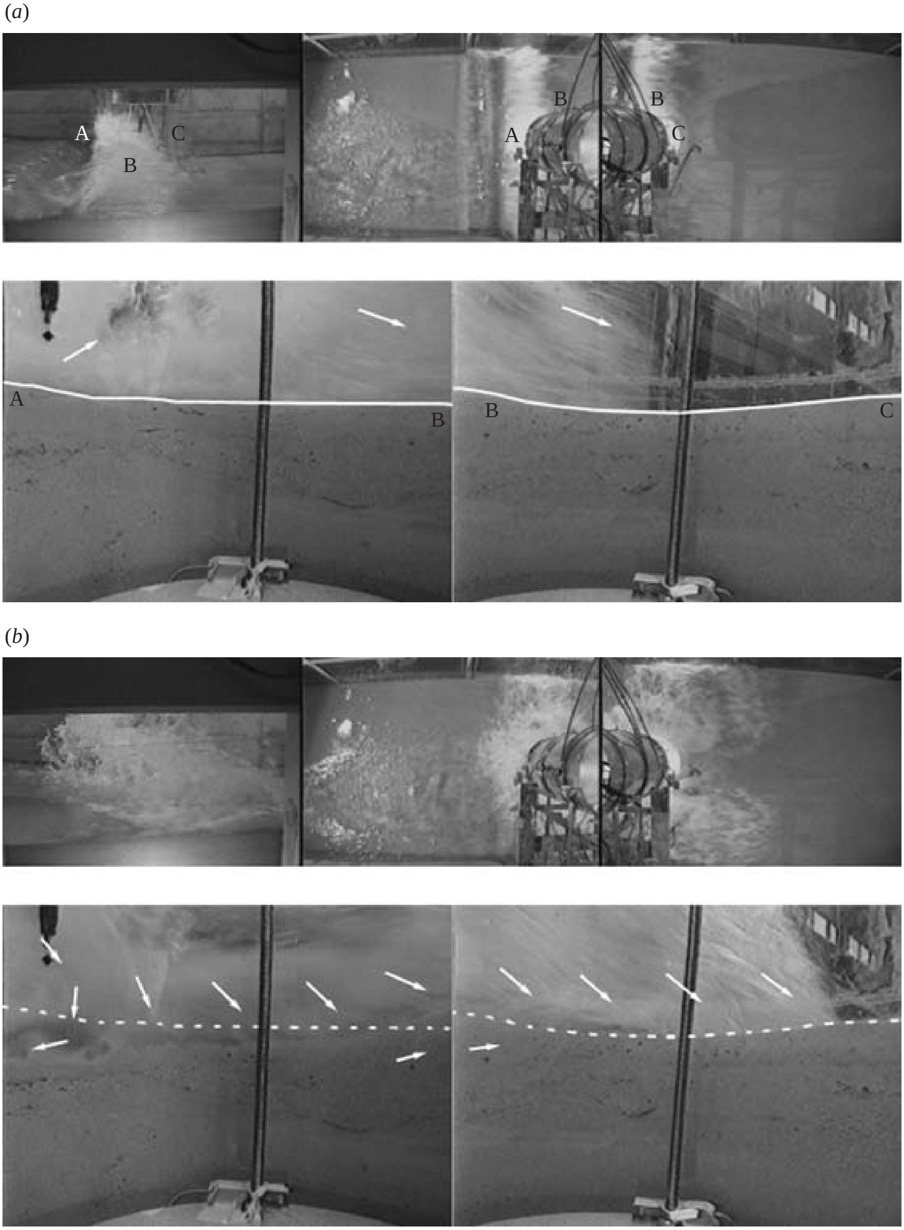

FIGURE 6(*a*, *b*). For caption see facing page.

opposite to the pore pressure and wave height sensors at the side of the cylinder. We assume cross-shore symmetry throughout, meaning that point B is taken to coincide with the sensors at the side.

Figure 6(*b*) shows the situation 0.25 s later. At the front of the cylinder, a downward flow pattern that resembles a horseshoe-type vortex has formed and is rapidly creating a localized scour hole. Unlike the steady flow situation of a bridge pier in which the horseshoe-type vortex is generated by the bottom boundary layer, here the plunging breaker and associated overturn just before the cylinder are responsible for generating

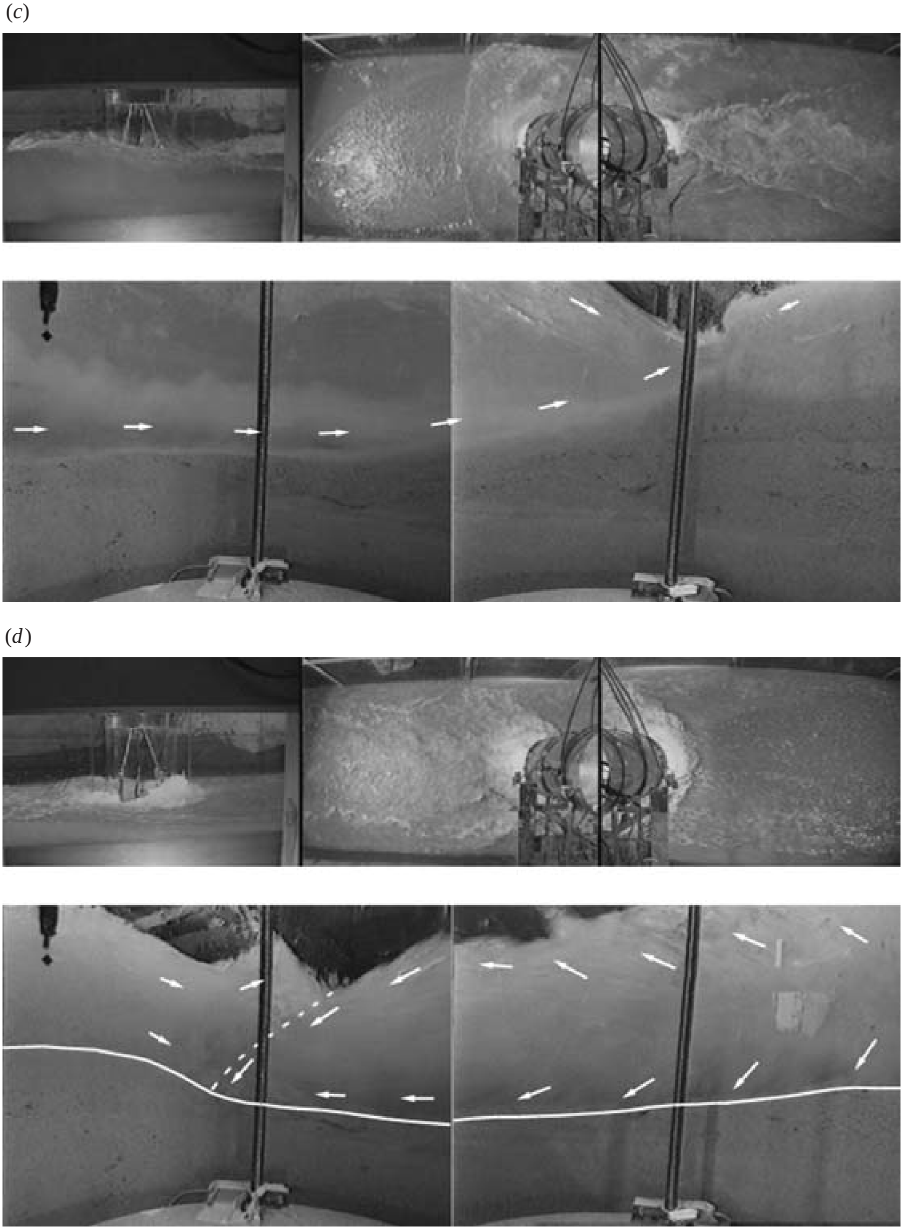

FIGURE 6. Video images showing a 22 cm wave incident on the cylinder embedded in sand at the shoreline (Case I). Top left panel: side view; top right panels: directly from above; bottom panels: from inside the cylinder. The flow field as it relates to sediment motion is suggested through arrows. (*a*) Situation at the moment that the wave impinges on the cylinder. The initial sediment level is outlined with a white line. The view from above, in the upper right panel, has an overlap such that the single bore appears twice. (*b*) 0.25 s after the initial wave impact, early in the wave runup. The initial sediment level is outlined as a broken line. (*c*) 2 s after the initial wave impact, during the main wave runup. (*d*) 14 s after the initial wave impact, during the most turbulent part of the wave drawdown. The broken line shows the position of a well-defined vortex sheet; the flow is generally upward to the left of this sheet and downward (as shown) to the right.

the clockwise vortex. The vortex is bent around the cylinder to form the observed horseshoe-type vortex; significant velocity shear associated with the large coherent vortex can cause scouring.

The shear stress at the side of the cylinder is very large. As indicated by the arrows, sediment is being brought into suspension around the side of the cylinder. The sediment skeleton in this region is also being sheared – in several places, larger pores (visible between the sand grains) are visibly deforming at this time.

Two seconds after the initial wave impact – and during the main wave runup – the horseshoe-type vortex is no longer visible in the fully developed runup flow field (figure 6*c*). Scouring continues, but more slowly, at the front and side of the cylinder; the scour hole is about 10 cm deep at this time, and there is a visible layer of suspended sediment at the front (although not at the side) of the cylinder. (The suspended sediment was presumably transported from offshore.) The dominant scour mechanism at the side of the cylinder is associated with the flow separation at the confluence of the main-flow and wake regions: strong upward flow is generated by flow convergence. Additional vorticity is created at the flow separation point by the pressure gradient along the bed and cylinder surface. The scoured sediments are transported away into the main flow. Note that the upper right-hand panel shows a reflected wave moving offshore from the cylinder.

About 6 s after the initial wave impact (not shown), the runup ends and the water motion pauses throughout the observable area. The scour hole is about 7 cm in depth around the front and the side of the cylinder, primarily caused by the initial horseshoe-type vortex created by the wave breaking in front of the cylinder.

During the drawdown, the situation becomes much more complex and turbulent as shown in figure 6(*d*), 14 s after the initial wave impact. There are significant differences between this drawdown flow and the well-developed runup flow shown in figure 6(*c*). The water moving directly towards the back of the cylinder is forced down, toward the sediment, in the lower half of the water column. This creates a counter-clockwise horseshoe-type vortex at the bed. Clockwise vortices are generated near the water surface, associated with the surface rollers. A great deal of scour is occurring at the back (onshore side) of the cylinder. A rapid and significant suspension of the sediments takes place between 13 s and 17 s after the initial wave impact: the scouring process is about one-quarter completed in figure 6(*d*). The water level at the back of the cylinder is decreasing rapidly during this period, and as described later this causes a rapid decrease in the bottom pressure and so in the effective stress between the sand grains. This decreased effective stress allows for very rapid scouring.

A vortex sheet – indicated by the broken line in figure 6(*d*) – forms at the wake separation point, and scouring continues here. The separation point is extremely turbulent; multiple small vortices form and disappear along the vortex sheet, with an individual lifetime of approximately 0.3 s. The main flow is generally downward along the vortex sheet, while the secondary flow (offshore) is generally upward.

At the end of the drawdown, the maximum scour depth – at the back of the cylinder – is about 15 cm. When the sediment finally settles it fills the scour hole to about one-half of its maximum depth. Figure 7 shows the observed scour depth at the cylinder wall as a function of time, indicating that this settlement occurs within less than a second (between 18 and 19 s).

3.2. *Case I, sand substrate: wave heights, velocities and pore pressures*

The horizontal and vertical velocities and the wave height were measured 3 m offshore from the cylinder. Figure 8 shows the wave height and horizontal velocity for Case I.

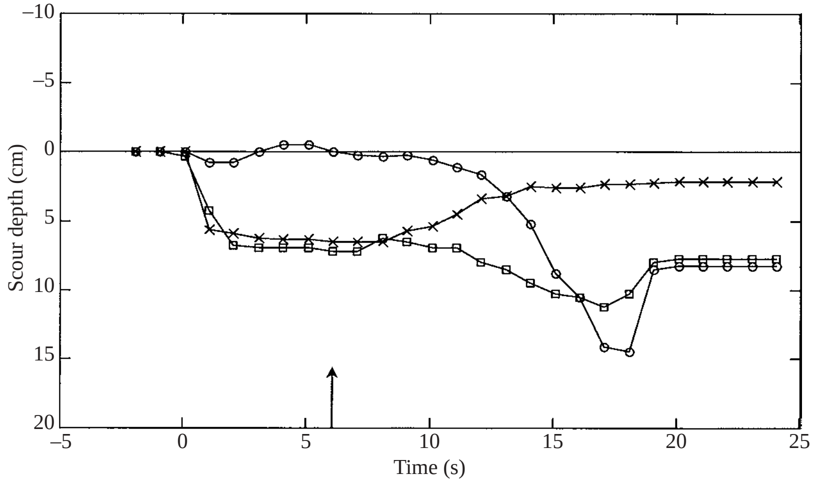

FIGURE 7. Scour depth as a function of time for Case I. Crosses, at the front of the cylinder; squares, at the side; circles, at the back. The arrow indicates the time of flow reversal, 6 s after wave impact.

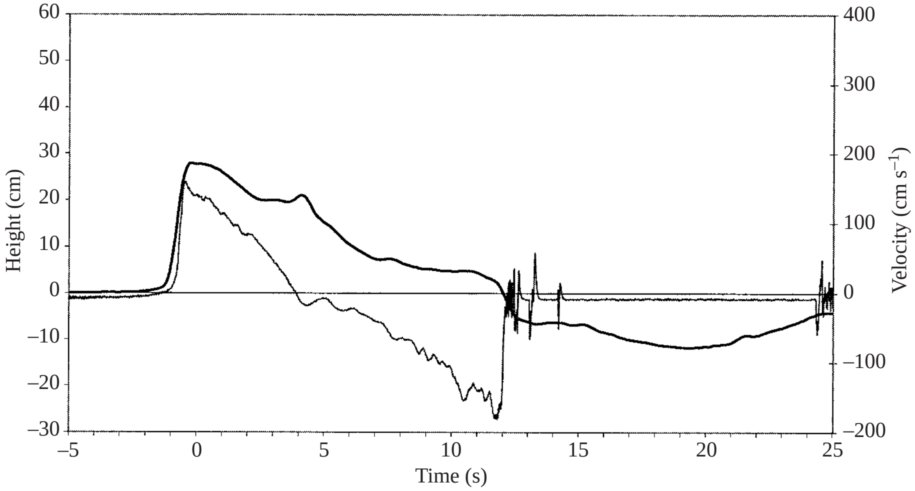

FIGURE 8. Wave height (thick line) and horizontal velocity (fine line) for Case I measured at the runup point, 3 m offshore from the cylinder. The origin of the time scale is at the initial wave impact at the front of the cylinder.

The measured wave height and velocity match those in the video images. The reflected wave, visible 2 s after the initial wave impact in the upper panel of figure 6(*c*), is visible in figure 8 as a local increase in the wave height 3 m offshore about 4 s after wave impact. The water velocity drops approximately linearly from its initial peak during the runup, and it grows linearly during the first part of the drawdown. It is close to zero about 4 to 6 s after the wave impact; this corresponds to the end of the runup. During the most turbulent part of the drawdown, from 13 s to 17 s after the initial wave impact, the water level is too low to give a valid velocity measurement; the sensor is not fully submerged at this point. However, visual observations of the

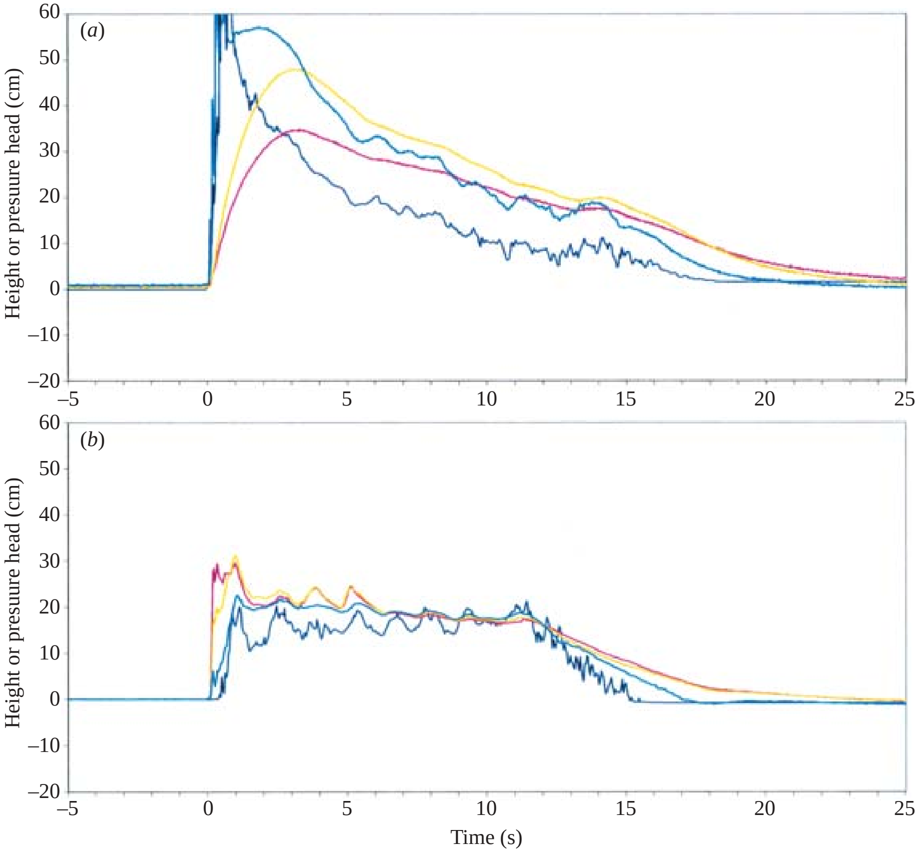

FIGURE 9. Wave height (blue line), and pore pressure heads at 10 cm (cyan), 20 cm (yellow) and 30 cm (pink) depth, measured for Case I: (*a*) at the front of the cylinder, (*b*) at the back of the cylinder.

flow field suggest that the magnitude of the water velocity is decreasing near the end of the drawdown as much of the wave energy is dissipated in friction and in turbulent fluctuations, and this is consistent with other water velocity measurements discussed later.

Figure 9 shows the measured wave height and pore pressure heads at 10 cm, 20 cm and 30 cm depth at the front and the back of the cylinder. These quantities are shown relative to their initial values, and in equivalent units – the pore pressures are expressed as the pressure heads, i.e. the pressure per unit weight of water. (Note that in figure 9, the wave height on impact ($t = 0$) exceeded the wave-gauge length of 60 cm).

Most of the scour at the back of the cylinder occurs from about 13 to 17 s after the initial wave impact (figure 7). This is the end of the drawdown period, when the water level and associated dynamic pressure have dropped from their previous level. As shown in figure 9(*b*), the pore pressure at 10 cm depth drops more rapidly than the pore pressure heads at 20 cm and 30 cm, so a pore pressure gradient builds up, decreasing the effective stress between the sand grains, and making the sand more susceptible to scour. The greatest pore pressure gradient seen in figure 9(*b*) corresponds to a difference in pressure head of 4 cm between pressure sensors 10 cm apart – a vertical gradient of −0.4 in the pore pressure head. As described later (see equation (3)), the sediment would liquefy – providing no resistance to scour – if the gradient in the pore pressure head reached −0.93. Figure 9(*b*) is typical of all similar cases examined, in that the occurrence of rapid scour coincides with the maximum pore pressure gradient, at approximately one-half the gradient required for sediment liquefaction.

The pressures above the sediment level are not hydrostatic here. One way to estimate the dynamic portion of the pressure is from the vertical flow velocity in front of the cylinder. Video images from Case II, for example figure 10(*a*), can be used to estimate this. The downward motion of a single piece of gravel during a single video frame is seen as a streak several centimetres long; the downward speed of the gravel, assumed to move with the flow field, can be estimated from the length of this streak and the frame rate. For the first 2 s after the wave impinges on the cylinder, the resulting downward velocities lie between 180 and 420 cm s^{-1}, comparable to the measured free-stream velocity (figure 8).

The corresponding dynamic pressure head, $v^2/2g$, is estimated at 30 to 90 cm. This (very approximate) estimate shows that the total pressure head at the top of the sediment in the first few seconds after impingement can be significantly greater than the water level. This explains how it is possible for the pore pressure head to be significantly above the water level in the first two seconds of the run, as shown in figure 9(*a*).

3.3. *Case II, gravel substrate*

Case II is identical to Case I, except that the substrate is gravel rather than sand: the cylinder is initially on the shoreline ($h = 2.45$ m) and the offshore incident wave height is 22 cm ($H/h = 0.09$). During much (but not all) of the passage of the wave, the large gravel grains move as bedload rather than the suspended load seen in Case I. Additionally, the permeability of the gravel is much higher than that of the sand, so the gravel cannot sustain large pore pressure gradients, which are not, therefore, available to contribute to rapid scour during the wave drawdown.

Figure 10 illustrates the flow and scour behaviour for Case II. Unlike figure 6, the upper right-hand pane shows the cylinder at an oblique angle, looking offshore. One second after wave impact (figure 10*a*) a substantial scour hole has formed at the front of the cylinder. Just as Case I, a visible horseshoe-type vortex is generated by the breaking wave. The behaviour of the gravel at the wake separation point is quite different from that of the sand in Case I, however. As in Case I, a reverse flow is present in the wake region, and the water level is lower in the wake than it is in the main flow. The resulting upward movement of the main flow at the separation point is not strong enough to bring the large gravel grains into suspension. Instead, the gravel moves as bedload – the grains roll toward the back of the cylinder, and at times migrate coherently as small dunes. This leads to significant accretion of gravel at the back of the cylinder; the sediment level at this time is higher than the starting level indicated by the broken line in figure 10(*a*). By the end of the runup, the gravel forms an almost straight-line profile, apparently at the angle of repose.

Figure 10(*b*) shows the situation as the drawdown becomes turbulent. At the back (onshore side of the cylinder), the gravel that was previously piled above the level of the front scour hole moves down as bedload into that scour hole; the level of gravel around the cylinder becomes nearly flat. The water at the back of the cylinder is nearly clear: while the flow around the cylinder back is strong enough to move bedload, it is not strong enough to bring the gravel into suspension. Even during

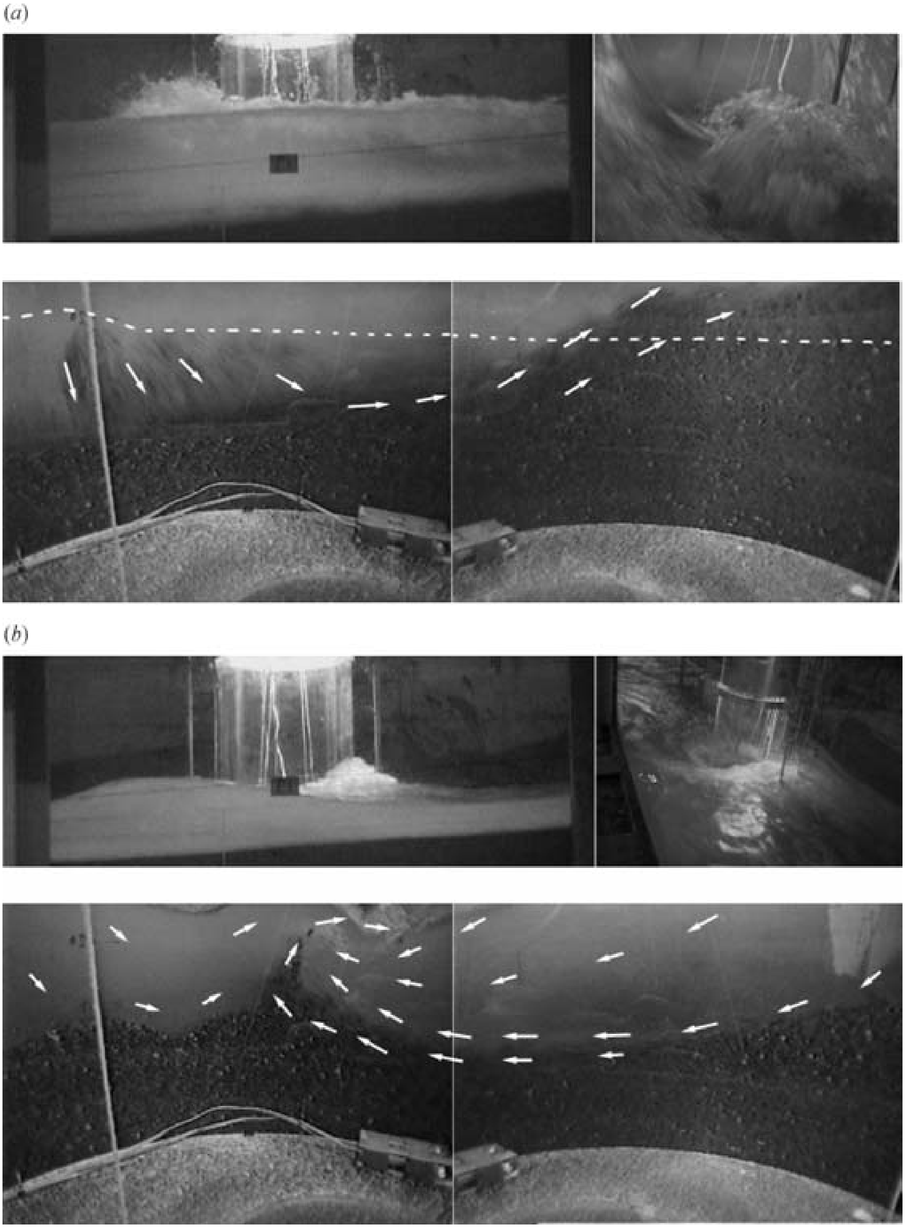

FIGURE 10(*a*, *b*). For caption see facing page.

the most turbulent parts of the drawdown, when a well-developed horseshoe-type vortex is scouring the gravel at the back of the cylinder, the rate of scour is rather small.

At the side of the cylinder, a well-defined vortex forms at the wake separation point. This vortex is strong enough to bring gravel into suspension, allowing some of the gravel moved to that point as bedload to be transported away. This vortex represents the only mechanism strong enough to bring the gravel into suspension during the entire runup-drawdown event.

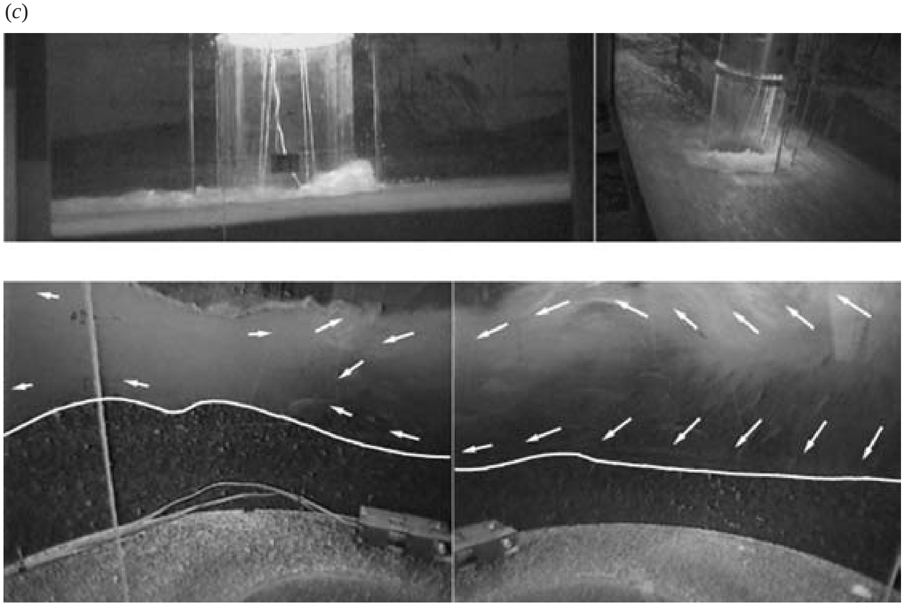

FIGURE 10. Video images showing a 22 cm wave incident on the cylinder embedded in gravel at the shoreline (Case II). Similar to figure 6 but the upper right-hand panel shows the cylinder at an oblique angle. The flow field as it relates to sediment motion is suggested through arrows. (*a*) 1 s after the initial wave impact, during the main wave runup. The initial sediment level is shown as a broken line. There is significant bedload transport in this run; the lower arrows on the right-hand side indicate bedload. (*b*) 12 s after the initial wave impact, during the most turbulent part of the wave drawdown. As in the runup, much of the sediment transport is in the form of bedload. (*c*) 14 s after the initial wave impact near the end of the wave drawdown. The sediment level at this time is outlined.

During the final 2 s of the flow pattern, shown in figure 10(*c*), the water level is dropping rapidly and the water velocity is also starting to drop. The scour hole at the back of the cylinder is being filled in during this period. This is in marked contrast to the situation with a sand substrate (Case I), where rapid scour continued to occur through this period. Because of the high permeability of the gravel substrate, it is not possible for a significant pore pressure gradient to build up as the water level drops – any such gradient would dissipate immediately. This means that the horseshoe-type vortex does not have the advantage of a pore pressure gradient in causing rapid scour during the final moments of drawdown.

Figure 11 illustrates the scour depth along the cylinder wall as a function of time for Case II. In contrast to Case I (sand substrate) shown in figure 7, the scour hole at the front and side of the cylinder are as deep as the scour hole at the back, and the scour hole at the back fills in, rather than continuing to scour, during the last few seconds of drawdown.

Figure 12 shows the wave height and pore water pressure heads at the front and the back of the cylinder. The wave height is similar to that shown in figure 9 for Case I (sand substrate). However, the pore pressure heads in gravel follow the wave height, and each other, much more closely than they do in sand. The measured pore pressures are not exactly equal to the total (hydrostatic plus dynamic) pressure at the top of the gravel, simply because this is not a one-dimensional situation. The

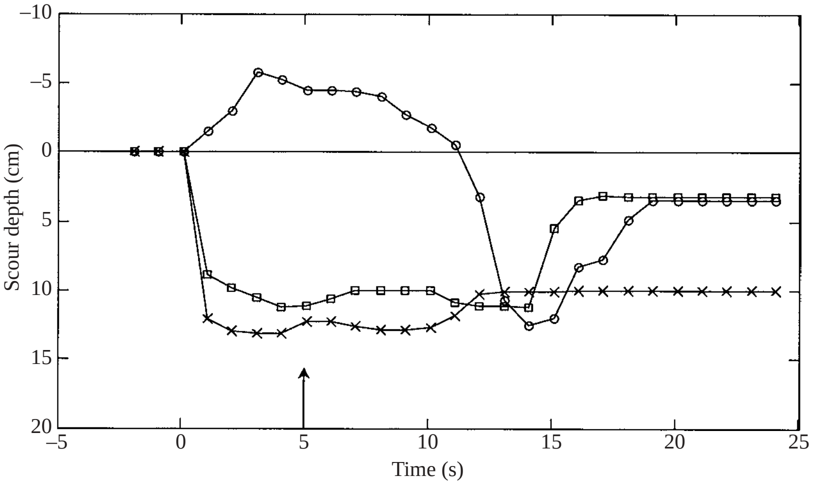

FIGURE 11. Scour depth as a function of time for Case II. Crosses, at the front of the cylinder; squares, at the side; circles, at the back. The arrow indicates the time of flow reversal, 5 s after wave impact.

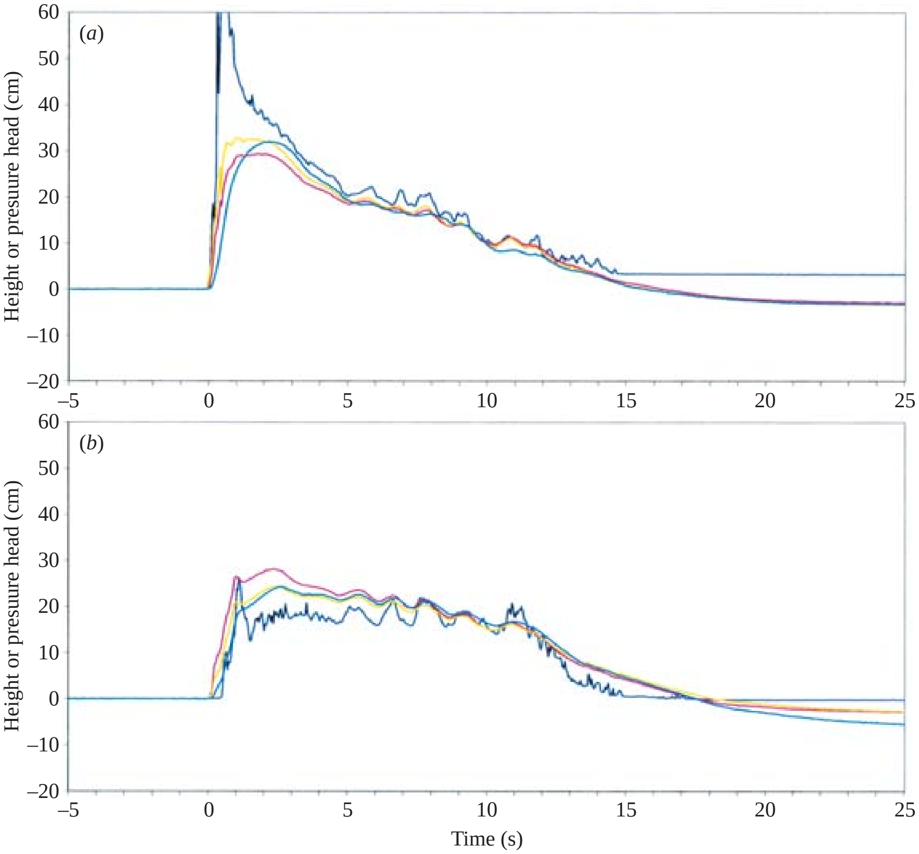

FIGURE 12. Wave height (blue line), and pore pressure heads at 10 cm (cyan), 20 cm (yellow) and 30 cm (pink) depth, measured for Case II: (*a*) at the front of the cylinder, (*b*) at the back of the cylinder.

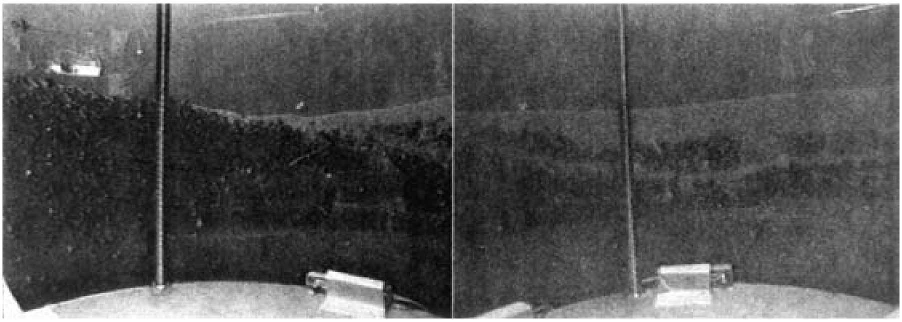

FIGURE 13. Additional gravel run after the wave has passed and the sediment settled.

surface pressure, and consequently the pore pressures, vary around the cylinder; for example, the surface pressure is lower in the wake.

At the back of the cylinder, figure 12(*b*) shows that a pore pressure gradient is set up only in the first few seconds after the initial wave impact. The pressure head at 30 cm depth increases more rapidly than at 20 cm and 10 cm. It appears that the high pressure induced by the wave impact at the front of the cylinder propagates through the gravel substrate underneath the cylinder; this is supported by measurements of pore pressure beneath the cylinder (not shown). This pore pressure gradient is evidently insufficient to cause scour; accretion due to bedload transportation from the side of the cylinder dominates. In contrast to Case I, no significant pore pressure gradient develops at the back of the cylinder during the last few seconds of the drawdown – the effective stress in the gravel does not decrease significantly at the end of the drawdown.

An interesting final condition is seen in figure 13. This gravel run is identical to Case II except that the cylinder was initially at a still water depth of 20 cm. The sediment finished with layers of sand and gravel within the filled scour hole. This demonstrates that a single wave runup/drawdown process is capable of creating a multiple-layered sediment deposit.

3.4. *Case III, additional sand substrate example*

Figure 14 illustrates Case III, the second sand substrate example: cylinder initially offshore ($h = 2.65$ m) and the offshore incident wave height 34 cm ($H/h = 0.13$). The main differences compared to Case I occur during runup.

As shown in the upper left-hand panel of figure 14(*a*) taken 0.25 s after wave impact, the wave is not broken but is overturning when it reaches the cylinder, and the initial flow near the cylinder does not appear to be particularly turbulent. No visible horseshoe-type vortex has formed. As a result, less scour occurs immediately after impact compared to the smaller wave impinging on the cylinder at the shoreline (figure 6*b*), in which a horseshoe-type vortex was formed by the plunging breaker in front of the cylinder.

Through most of the runup, significant scouring occurs at the side of the cylinder. The fully developed runup flow field is illustrated in figure 14(*b*). At the side of the cylinder, a large amount of sediment is being entrained. A well-defined clockwise vortex is visible at the separation point, where the main forward flow and the reverse flow at the back of the cylinder meet. The main flow and the vortices with it are forced up and away from the bottom boundary. This upward motion drives the sediment uptake in this region. In contrast, the flow at the upstream stagnation point appears

(*a*)

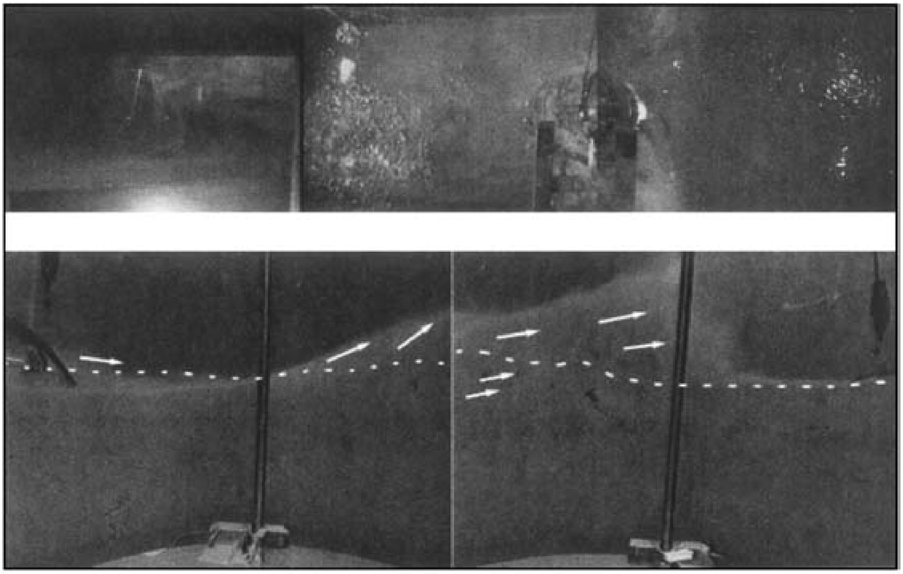

(*b*)

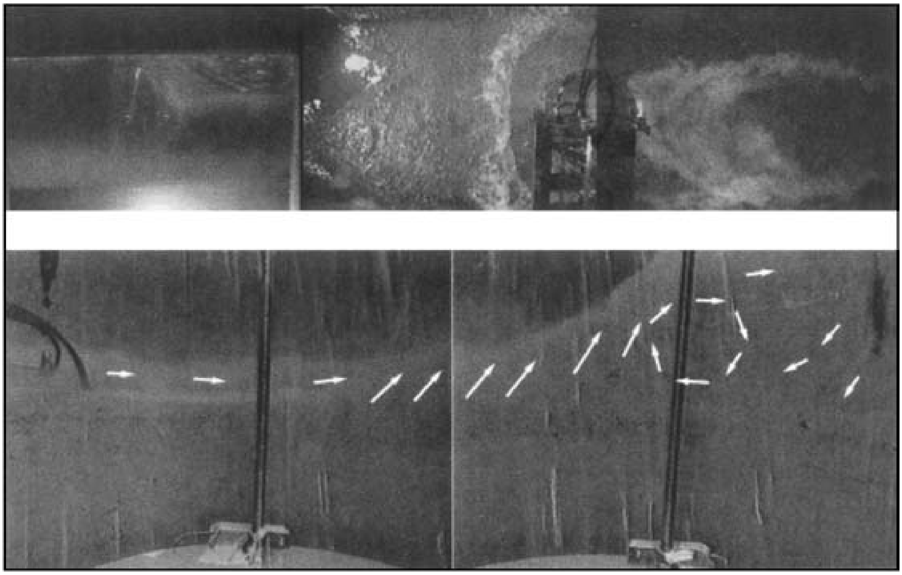

FIGURE 14. Video images showing a 34 cm incident on the cylinder embedded in sand offshore (Case III). The flow field as it relates to sediment motion is suggested through arrows. (*a*) 0.25 s after the initial wave impact. The initial sediment level is outlined as a broken line. (*b*) 1 s after the initial wave impact, during the main wave runup.

only slightly turbulent and no visible horseshoe-type vortex is present. Essentially no scour occurs at the stagnation point during this period, due to the absence of a well-formed horseshoe-type vortex; it may also be that the increasing surface pressure imposed by the incident wave tends to compact the sediment, increasing the effective stresses and strengthening the soil skeleton.

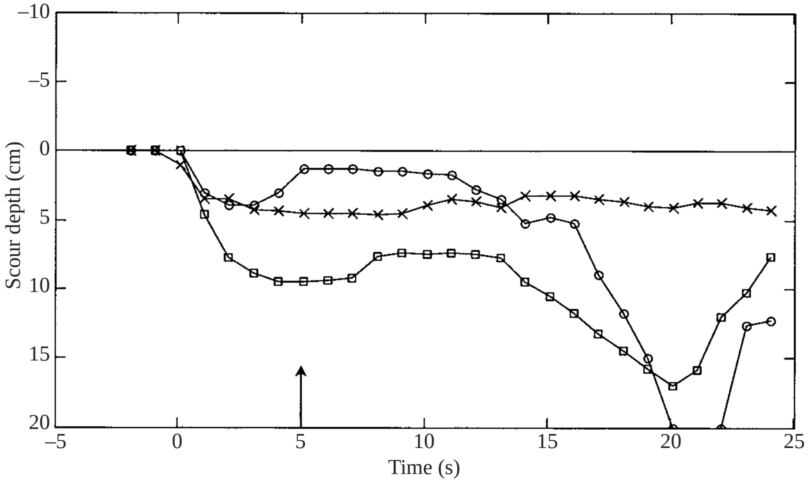

FIGURE 15. Scour depth as a function of time for Case III. Crosses, at the front of the cylinder; squares, at the side; circles, at the back. The arrow indicates the time of flow reversal, 5 s after wave impact.

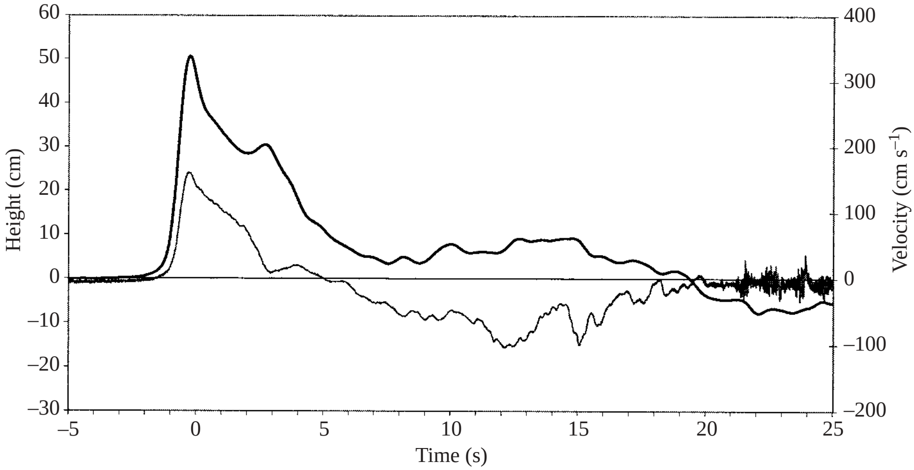

FIGURE 16. Wave height (thick line) and horizontal velocity (thin line) for Case III measured at the runup point, 3 m offshore from the cylinder. The origin of the time scale is at the initial wave impact at the front of the cylinder.

The flow field and scour mechanisms become more similar to Case I during drawdown (not shown); as indicated in figure 15, a great deal of scour occurs during the last few seconds of the drawdown.

Figure 16 shows the wave height and water velocity measurements for this run. As in the previous cases, the water velocity drops approximately linearly from its initial peak during the runup, and it grows linearly during the first part of the drawdown. Figure 16 shows that the magnitude of the water velocity decreases near the end of the drawdown as much of the wave energy is dissipated in friction and in turbulent fluctuations.

4. Scour mechanisms

4.1. *Observed scour rates*

The general behaviour of the flow field and the total depth of scour are similar for the experiments with and without gravel substrate. However, the temporal development of the scour hole at the back of the cylinder (onshore side) suggests different mechanisms for the sand substrate (figure 7) and the gravel substrate (figure 11).

(i) In the first second after the wave strikes, a large horseshoe-type vortex, originating from the overturning motion of the wave breaking offshore, is set up at the front of the cylinder. This vortex scours a hole about 3 cm to 7 cm deep for the sand substrate, about 13 cm deep for the gravel.

(ii) Throughout the runup, the sand scoured from the front and side of the cylinder is brought into suspension and carried away from the cylinder. In contrast, much of the gravel scoured from the front and side of the cylinder moves as bedload towards the back of the cylinder, accreting there to form a uniform slope, presumably equal to the angle of repose.

(iii) During the early part of drawdown, little sand is scoured from the back of the cylinder. In contrast, gravel returns down the slope at the back of the cylinder under the influence of drawdown, and is transported away by the strong vortex sheet at the wake separation point.

(iv) During the last few seconds of drawdown – the most turbulent period – a strong horseshoe-type vortex forms at the back of the cylinder. A very large quantity of sand is scoured from the back of the cylinder during this period, while the gravel scour hole actually fills in during this period.

There are strong similarities in the flow patterns for sand and gravel. The question therefore arises of why the horseshoe-type vortex that forms during the last few seconds of drawdown has such different effects on the sand and the gravel, rapidly scouring the sand while allowing the gravel hole to fill in. The following subsection shows that a standard shear stress model fails to elucidate this difference.

4.2. *Application of the Shields criterion*

The shear stress τ can be estimated in terms of the Shields parameter θ, its dimensionless form, using the formulation in Hoffmans & Verheij (1997):

$$\theta \equiv \frac{\tau}{gD_{50}(\rho_s - \rho_w)} \approx \frac{1}{gD_{50}} \frac{\rho_w}{\rho_s - \rho_w} \left[\frac{\kappa u}{\ln(30z/D_{90})} \right]^2, \tag{1}$$

where g is the acceleration due to gravity, D_{50} is the median sediment diameter, D_{90} is the 90th percentile of the sediment diameters, ρ_w is the density of water, ρ_s is the sediment grain density, $\kappa = 0.4$ is the von Kármán constant and u is the horizontal flow speed at a height z above the surface. For the present experiments $z = 7.5$ cm, the elevation at which the velocity sensor measured the flow velocity.

The flow velocity u was measured 3 m offshore from the cylinder. Therefore the actual flow velocity (and so the Shields parameter) at the cylinder lags the measured velocity during runup, and may lead the measured velocity during drawdown. The origin of the time scale has been shifted (by less than 1 s) to account for the phase lag during runup. Thus, the Shields parameter at the cylinder may lead the Shields parameter displayed in figure 17 during drawdown. This lead is small: there are no discrepancies between the time-shifted measured velocity and the velocity as estimated (approximately) from the videos. See Tonkin de Vries (2001) for more details.

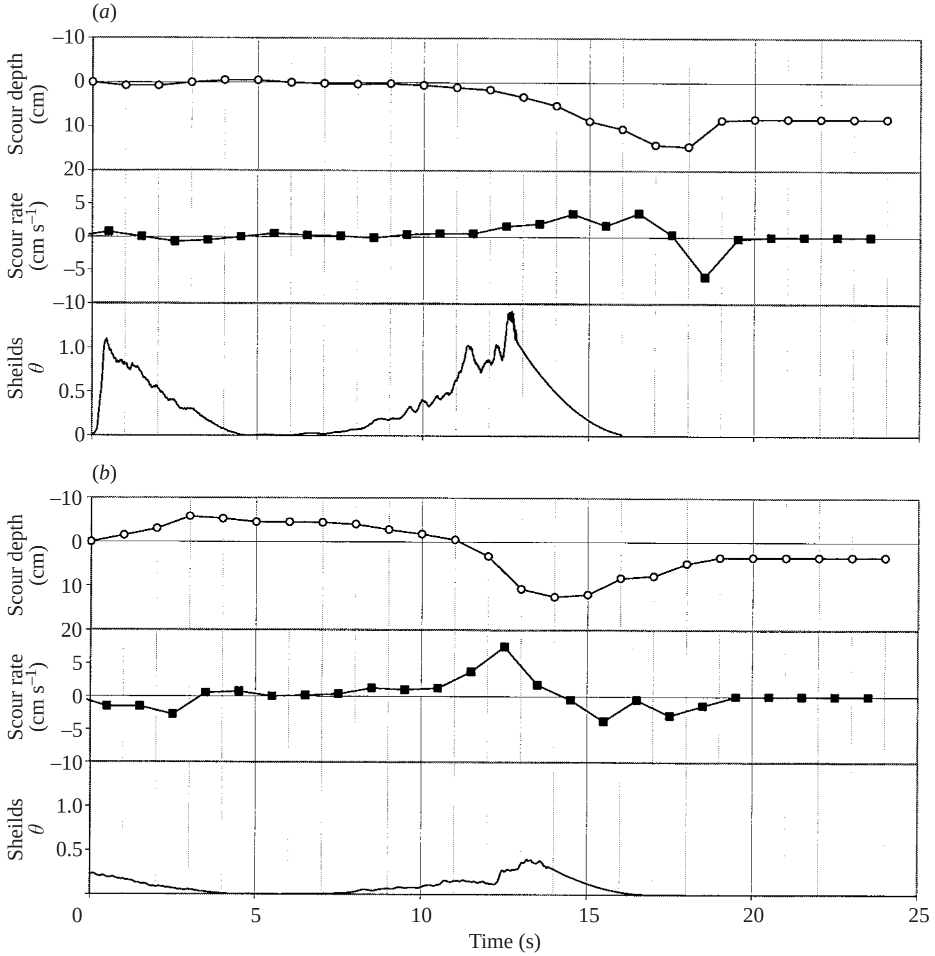

FIGURE 17. Measured scour depth, rate of scour and estimated Shields parameter for (*a*) Case I, (*b*) Case II.

This simplified shear stress model neglects such factors as the observed large-scale vortices and the extreme turbulence during drawdown; with a single velocity measurement, the shear stress at the sediment bed can only be estimated approximately. However, the observed flow during drawdown was similar for the sand and gravel substrates, so these factors should have similar effects for both substrates. In other words, if shear stresses at the sediment bed explain the scour rate for sand and gravel, this simplified model should work equally well (or badly) for both cases.

Figure 17 illustrates the Shields parameter θ (dimensionless shear stress) estimated from (1), together with the observed scour depth and the rate of scour at the back of the cylinder, for Cases I (sand) and II (gravel). For both cases, the shear stress peaks near $t = 0$, when the wave first reaches the cylinder; this is reflected by rapid scour at the front of the cylinder. Little scour occurs at the back of the cylinder at $t = 0$ due to the shadowing caused by the cylinder.

The shear stress has another peak during drawdown, at between 10 and 16 s for both the sand and the gravel. The flow velocity and (consequently) the shear stress drop to zero in the 2-3 s following this peak. For the gravel (figure 17*b*), most of the scour at the back of the cylinder occurs while the estimated shear stress is increasing, at between 11 and 14 s. It is clear from the videos that the sediment load transported from further onshore becomes extremely high after this period (see for example figure 10*c*). Thus, most of the scour at the back of the cylinder occurs while the shear stress is high and the sediment load is not exceptionally high – exactly as expected from shear stress models. If the actual velocity at the cylinder leads the velocity used to calculate θ (as discussed above) then the correlation between θ and the scour rate improves further.

In contrast, for the sand, most of the scour at the back of the cylinder occurs at between 14 and 17 s (figure 17*a*). During this time, the estimated shear stress is dropping rapidly and the sediment load transported from further onshore is observed to be increasing, so the scour rate would be expected to decrease. The main discrepancy between the predictions of the shear stress model and the observed scour rate is that the scour rate reaches its maximum at between 16 and 17 s, just as the flow velocity drops to zero. If the actual velocity at the cylinder leads the velocity used to calculate θ then the discrepancy increases further.

The time variation of the scour rate for gravel can easily be explained in qualitative terms using the present estimate of the Shields parameter (dimensionless shear stress). The time variation of the scour rate for sand, in a similar flow field, cannot be explained in this way. The critical point is that the scour rate for sand reaches its maximum as the flow velocity drops rapidly to zero. This basic observation highlights differences between the sand and the gravel, and casts doubt on the adequacy of the shear stress approach. In this paper we argue that the missing mechanism is the pore pressure gradient resulting from the rapid decrease in pressure as the wave withdraws.

4.3. *Enhanced scour due to pore pressure gradients*

The evolution of the pore pressure can be quantified in terms of Terzaghi's (1925) theory of soil consolidation (see Holtz & Kovacs 1981, for a more recent presentation). This theory is based on the concept of the excess pore pressure p_e (the pressure of the water within the sediment pores above the pressure expected hydrostatically):†

$$p_e(z,t) = p(z,t) - \rho_w g[h - z], \tag{2}$$

where the coordinate z is directed vertically upwards, p is the pressure relative to atmospheric and h is the water level. Terzaghi's theory shows that the sediment liquefies, with no effective stress between the sediment grains, if the vertical gradient in the excess pore pressure exceeds γ_b, the buoyant specific weight of the saturated soil skeleton:

$$\left.\frac{\partial p_e}{\partial z}\right|_{z=z_0} = -(\rho_{sat} - \rho_w)g \equiv -\gamma_b, \tag{3}$$

where ρ_{sat} is the bulk density of the saturated soil skeleton and z_0 is the elevation of the movable sediment bed. From the data in table 1, ρ_{sat} is computed to be $1.93 \times 10^3\,\mathrm{kg\,m^{-3}}$, so the vertical gradient in the pore pressure required for liquefaction is $-9.12\,\mathrm{kPa\,m^{-1}}$; the corresponding vertical gradient in the pore pressure head is -0.93.

---

† The measured pore pressures shown in this paper are relative to the initial hydrostatic pressure, not the time-dependent quasi-hydrostatic pressure; thus they are not the same as excess pore pressures. However, the vertical gradient in the measured pore pressure equals the vertical gradient in the excess pore pressure.

Large vertical pore pressure gradients can be expected to contribute to high scour rates. According to the traditional shear stress approach, sediment motion occurs when the lift and drag induced by the fluid motion overcome the resisting frictional and gravitational forces on a sediment grain. If the sediment liquefies, no resisting forces remain, and the sediment scours very readily. If the pore pressure gradient is a significant fraction of that required for liquefaction, in other words if a significant fraction of the buoyant weight of the sediment is supported by the pore pressure gradient, then the resisting forces are decreased by a significant fraction, and the scour rate can be expected to increase significantly.

In the present sequence of experiments, the largest measured gradients in the pore pressure heads were in the range -0.4 to -0.5 for sand – about one-half of that required for liquefaction. No significant pore pressure gradients were sustained in the gravel. The peak scour rates for sand at the back of the cylinder were typically coincident with the maximum pore pressure gradients. This is seen in figure 9(*b*), when the greatest pore pressure gradients (up to -0.4) occur at 14 to 16 s, and the greatest scour occurs at 14 to 17 s. Interestingly, Sumer *et al.* (1999) found that pipes tended to settle into a sediment (silt) bed when a cyclic buildup of pore pressures reached a gradient approximately half that required for liquefaction. This is a very different physical situation, but it can be conjectured that the structure of a sediment skeleton may change when this pore pressure gradient is reached.

We define a scour enhancement parameter $\Lambda(z)$ as the fraction of the buoyant weight of the sediment supported by the pore pressure gradient:

$$\Lambda(z) = \frac{p_e(z) - p_e(z_0)}{\gamma_b |z - z_s|}, \tag{4}$$

where $z_0 > z$ is the elevation at the top of the sediment bed. Λ is also the fraction by which the pore pressure gradient decreases the frictional forces resisting scour. For any given flow characteristics (depth, speed and vortex structure), there is some value of Λ for which the remaining frictional forces are small enough that scour occurs very rapidly. This threshold value of Λ must lie between 0 and 1; it takes a value of approximately 0.5 for the present experiments (e.g. figure 9*b*). We propose that rapid scour is anticipated to a depth z such that

$$\Lambda(z) \geqslant \Lambda_T, \tag{5}$$

where Λ_T is the threshold value of Λ.

4.4. *Prediction of enhanced scour*

To predict the depth of enhanced scour using only basic wave and substrate characteristics, we apply Terzaghi's (1956) model of the dissipation of excess pore pressures:

$$\frac{\partial p_e}{\partial t} = c_v \frac{\partial^2 p_e}{\partial z^2}, \tag{6}$$

where c_v is Terzaghi's coefficient of consolidation. Equation (6) assumes a one-dimensional system, an elastic soil skeleton (corresponding to small strains) and saturated pores. If the pores are not fully saturated then, based on the formulation of Jeng & Hsu (1996), a similar equation holds with a modified value of c_v. This equation represents a simplification of the present experiments, since the pressure field is not purely one-dimensional and the sand skeleton is not completely elastic. However, it provides significant insight into the physical situation.

Condition (5) for the occurrence of enhanced scour will be satisfied if the surface pressure drops by a sufficiently large amount ΔP in a sufficiently short time ΔT during the drawdown. Two criteria for the depth d_s of enhanced scour can be deduced from (4)–(6):

(i) The time scale ΔT must be short enough that the rate of diffusion, defined through c_v, is insufficient to allow the pore pressure gradient to dissipate over a depth d_s.

(ii) The total drop in pressure ΔP must be at least as large as $\Lambda_T \gamma_b d_s$, in order that a gradient $\Lambda_T \gamma_b$ in the excess pore pressure can be maintained through the vertical distance d_s.

In other words, the scour depth d_s must obey

$$\sqrt{c_v \Delta T} < d_s < \frac{\Delta P}{\Lambda_T \gamma_b}. \tag{7}$$

If these criteria are inconsistent then no enhanced scouring should occur.

To quantify this further, assume that the pore pressures at the back of the cylinder are hydrostatic at the end of the runup; the sediment bed is immobile with the surface remaining at $z_0 = 0$; and that the excess pore pressure at $z_0 = 0$ drops linearly by ΔP in a time ΔT during drawdown. This linear decrease is supported by observations, as described below. At the end of this time, based on the diffusion equation (6), the pore pressures are given by (Carslaw & Jaeger 1959)

$$p_e(z) = 4\Delta P \mathrm{i}^2\mathrm{erfc}\left[\frac{-z}{2\sqrt{c_v \Delta T}}\right], \tag{8}$$

where $\mathrm{i}^2\mathrm{erfc}[\cdot]$ is the second integral of the complementary error function:

$$i^2\mathrm{erfc}(x) = \int_x^\infty \mathrm{d}x' \int_{x'}^\infty \mathrm{d}x''\mathrm{erfc}(x''). \tag{9}$$

Since

$$p_e(-d_s) - p_e(0) \equiv \Lambda(d_s)\,\gamma_b\, d = \Delta P\left(1 - 4\mathrm{i}^2\mathrm{erfc}\left[\frac{d_s}{2\sqrt{c_v \Delta T}}\right]\right), \tag{10}$$

the scour enhancement parameter at depth d_s is given by

$$\Lambda(d_s) = \frac{\Delta P}{\gamma_b\, d_s}\left(1 - 4\mathrm{i}^2\mathrm{erfc}\left[\frac{d_s}{2\sqrt{c_v \Delta T}}\right]\right). \tag{11}$$

This solution replaces the order-of-magnitude criteria of (7) by a quantitative measure of whether enhanced scour is expected to a given depth d_s. If $\Lambda(d_s)$ exceeds Λ_T then enhanced scour is anticipated at d_s. Taking the limit as $d_s \to 0$ yields a measure of whether any enhanced scour can occur:

$$\Lambda(0) = \frac{2}{\sqrt{\pi}}\,\frac{\Delta P}{\gamma_b \sqrt{c_v \Delta T}}. \tag{12}$$

For the gravel substrate, c_v is very large, no significant pore pressure gradient can be sustained and enhanced scour does not occur.

The fact that the gravel scours more readily than the sand at the front of the cylinder may also result in part from pressure gradient effects. When the wave first impacts the cylinder, a sudden increase in water pressure on the sand bed creates a

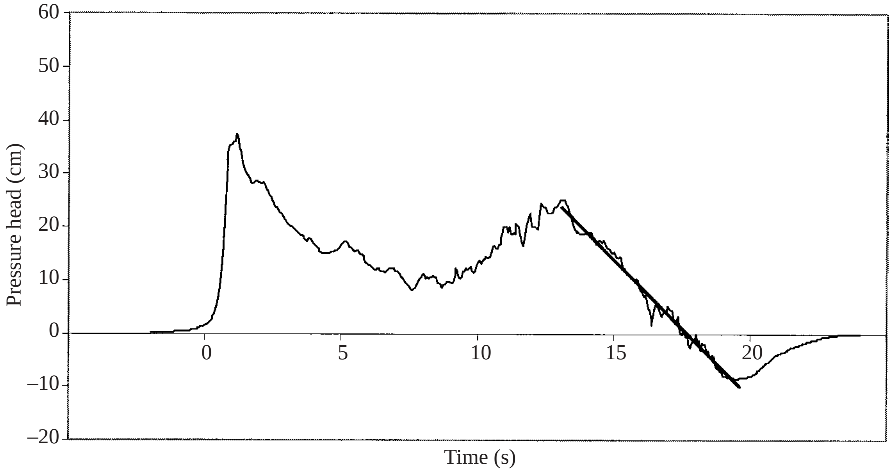

FIGURE 18. Linear fit to the drawdown portion of the pressure head at the back of the cylinder.

pore pressure gradient such that the effective normal stress increases in the sediment, and resistance to scour increases. This pore pressure gradient that resists scour cannot be established in the gravel bed.

4.5. *Application*

To apply criteria (11) and (12) to the present experiments, we make the following approximate estimates of ΔP, ΔT and c_v.

Flow characteristics ΔP *and* ΔT. We use Baker's (1979) result that the total pressure at the front of a cylinder in steady flow is equal to the hydrostatic pressure for an undisturbed flow, plus the dynamic pressure $\rho v^2/2$ where v is the undisturbed flow velocity. The modelled total pressure is well fitted by a straight line during drawdown; see for example figure 18. The hydrostatic pressure head is calculated from the wave height measured between the cylinder and the sidewall (relatively undisturbed) and the dynamic pressure from the flow velocity measured 3 m offshore.

The consolidation coefficient c_v. Using data from standard geotechnical tests applied to the present sand specimen (Tokyo Soil Research 1999) and the small-strain model of Hicher (1996), we obtained the value $c_v = 0.08\,\mathrm{m^2\,s^{-1}}$: see Tonkin de Vries (2001) for more details. This estimate is supported by laboratory measurements by Heller (2002), who found values of c_v between 0.06 and $0.10\,\mathrm{m^2\,s^{-1}}$ for sand in the low-pressure range. Heller measured pore pressures in sands contained in a stiff vertical cylinder. The pressure at the sand surface was released by discharging water though an orifice placed above the surface. The value of c_v was computed using (6).

Table 2 gives the resulting predictions for the scour enhancement parameter at the sediment surface, $\Lambda(0)$, and the scour enhancement parameter at the maximum observed scour depth, $\Lambda(d_s)$. The results shown in table 2 indicate that $\Lambda(0)$ lies below 0.5 for those cases where relatively shallow scour holes are formed: at the front of the cylinder, and for the smaller (13 cm) wave at the back of the cylinder. $\Lambda(0)$ lies slightly above 0.5 for the three cases where a deep scour is observed during drawdown. The results support our conjecture $\Lambda_T \approx 0.5$, and are consistent with the observed pore pressure gradients as shown in figure 9(*b*).

h (m)	H (m)	ΔT (s)	ΔP (kPa)	ΔH_p (m)	$\Lambda(0)$	Measured scour depth d_s (m)	$\Lambda(d_s)$
Values at cylinder front							
2.65	0.13	4.5	1.28	0.13	0.26	0.000	–
2.65	0.24	6.5	1.77	0.18	0.30	0.025	–
2.65	0.34	6.0	1.96	0.20	0.35	0.043	–
2.45	0.22	3.0	1.37	0.14	0.35	0.024	–
Values at cylinder back							
2.65	0.13	4.5	1.67	0.17	0.35	0.026	–
2.65	0.24	6.5	3.34	0.34	0.57	0.144	0.52
2.65	0.34[1]	6.5	3.63	0.37	0.62	>0.2	<0.55
2.45	0.22[2]	6.5	3.34	0.34	0.57	0.145	0.52

[1]Case III described previously. [2]Case I described previously.

TABLE 2. Calculation of the scour enhancement parameter based on a linear fit to the drawdown pressure head ΔH_p.

5. Summary and conclusions

Scour mechanisms associated with a tsunami impinging on a vertical cylinder were examined using a large-scale sediment tank: a tsunami is modelled as an incident solitary wave. The time development of the scour is likely to be critical in this transient situation. Visual observations elucidated the time development and some of the mechanisms of the scour.

The timing and occurrence of scour at the front and side of the cylinder for both sand and gravel substrates, and at the back of the cylinder for the gravel substrate, can be qualitatively explained in terms of the standard shear stress model (no quantitative explanation is attempted). However, the very rapid scour in the sand substrate at the back of the cylinder at the end of drawdown, when the flow velocity is decreasing rapidly and the sediment load is already high, cannot be explained in this way. This brief but very rapid scour creates the deepest, although transient, scour holes observed during the experiments.

This rapid scour can be explained by including the effects of pore pressures. The rapidly decreasing water level at the end of the drawdown brings about a pore pressure gradient. This pore pressure gradient buoys up the sediment near the surface, decreasing the frictional forces between the sediment grains and so decreasing the fluid velocity required to suspend the sediment through lift and drag forces. If the pore pressure gradient were high enough that the effective stress between the sediment grains vanished, the sediment would liquefy and scour extremely rapidly. This was observed in none the experiment runs discussed here; the gradients in the measured pressures never greatly exceeded one-half of that required for liquefaction. However, the pore pressure gradient does become large enough to support much of the weight of the sediment grains. It appears that this greatly enhances the scour rate.

A scour enhancement parameter Λ is proposed, defined as the fraction of the buoyant weight of the sediment grains that is supported by the pore pressure gradient. An explicit expression for Λ as a function of depth within the substrate, (11), is developed using basic flow and substrate characteristics. It was found that scouring occurred to a depth d_s such that one-half of the weight of the sediment grains was buoyed up by the excess pore pressure gradient, that is, such that the calculated value of Λ reached approximately 0.5. Explicit measurements of the pore pressure such as those shown in figure 9 support this conclusion: the most rapid scour occurred when the measured pore pressure gradient was at or above half that required for sediment liquefaction. The reason for the threshold value $\Lambda_T \approx 0.5$ is not clear, although we conjecture that it might be related to changes in the structure of a sediment skeleton.

This work was supported by Public Works Research Institute, the Japan Ministry of Construction, and the US National Science Foundation (CMS-9978399). Technical assistance of H. Watanabe throughout the experimental programs is acknowledged.

REFERENCES

Baird, A. J., Mason, T. E. & Horn, D. P. 1996 Mechanisms of beach ground water and swash interaction. In *Coastal Engineering 1996, Proc. 25th Intl Conf.* (ed. B. L. Edge), pp. 4120–4133.

Baker, C. J. 1979 The laminar horseshoe vortex. *J. Fluid Mech.* **95**, 347–367.

Breusers, H. N. C., Nicolet, G. & Shen, H. W. 1977 Local scour around cylindrical piers. *J. Hydraul. Res.* **15**, 211–252.

Carslaw, H. S. & Jaeger, J. C. 1959 *Conduction of Heat in Solids*. Oxford University Press.

Çevik, E. O. & Yüksel, Y. 1999 Scour under submarine pipelines in waves in shoaling conditions. *J. Waterway Port Coast. Ocean Engng* **125**, 9–19.

DePonte, S. & Monti, R. 1995 Flow field around a circular obstacle emerging from an erosion scour hole. In *Small-Scale Structures in Three-Dimensional Hydrodynamic and Magetohydrodynamic Turbulence, Proc. Nice, France* (ed. M. Meneguzzi, A. Pouquet & P.-S. Sulem), pp. 221–229. Springer.

Dey, S. 1999 Time-variation of scour in the vicinity of circular piers. *Proc. Inst. Civil Engnrs: Water, Maritime & Energy* **136**, 67–75.

Heller, E. W. 2002 Determination of the coefficient of consolidation for the prediction of enhanced scour near tsunamis. MS thesis, University of Washington, Seattle.

Hicher, P.-Y. 1996 Elastic properties of soils. *J. Geotech. Engng* **122**, 641–648.

Hoffmans, G. J. C. M. & Verheij, H. J. 1997 *Scour Manual*. A. A. Balkema, Rotterdam.

Holtz, R. D. & Kovacs, W. D. 1981 *An Introduction to Geotechnical Engineering*. Prentice Hall.

Jeng, D. S. & Hsu, J. R. C. 1996. Wave-induced soil response in a nearly saturated sea-bed of finite thickness. *Géotechnique* **46**, 427–440.

Madsen, O. S. 1978 Wave-induced pore pressures and effective stresses in a porous bed. *Géotechnique*, **28**, 377–393.

Mia, M. F. & Nago, H. 2000 Prediction of bed liquefaction and local scour around a bridge pier under abrupt water pressure change. In *Scour of Foundations: Proc. Intl Symp. International Society of Soil Mechanics and Geotechnical Engineering, Technical Committee TC-33*, (ed. J. L. Briaud), pp. 23–37.

Okusa, S. 1985 Wave-induced stresses in unsaturated submarine sediments. *Géotechnique* **35**, 517–532.

Sumer, B. M. & Fredsøe, J. 1999 Wave scour around structures. In *Advances in Coastal and Ocean Engineering* (ed. P. L. F. Liu), pp. 191–249. World Scientific.

Sumer, B. M., Fredsøe, J., Christensen, S. & Lind, M. T. 1999 Sinking/floatation of pipelines and other objects in liquefied soil under waves. *Coastal Engng* **38**, 53–90.

Sumer, B. M., Whitehouse, R. J. S. & Tørum, A. 2001 Scour around coastal structures: a summary of recent research. *Coastal Engng* **44**, 153–190.

Synolakis, C. E. 1987 The runup of solitary waves. *J. Fluid Mech.* **185**, 523–545.

Takahashi T., Imamura, F. & Shuto, N. 1992 Research on flows and bathymetry variations by tsunami: the Case of Kesen-numa Bay, Japan, due to the 1960 Chilean Tsunami. *Tsunami Engineering Tech. Rep.* 9, pp. 185–201, Tohoku University (in Japanese).

Terzaghi, K. 1925 *Erdbaumechanik*. Franz Deutike, Vienna (in German).

Terzaghi, K. 1956 Varieties of submarine slope failures. *Harvard Soil Mechanics Series* 52, Cambridge, MA.

Tokyo Soil Research 1999 *Soil Test Report for the Beach Model* (in Japanese).

Tonkin de Vries, S. P. 2001 Tsunami-induced scour around a vertical cylinder: an effective stress approach. MS thesis, University of Washington, Seattle.

Yeh, H., Kato, F. & Sato, S. 2001 Tsunami scour mechanisms around a cylinder. In *Tsunami Research at the End of a Critical Decade* (ed. G. T. Hebenstreit), pp. 33–46. Kluwer.